Journal of
Ceramic Science
and Technology

J. Ceram. Sci. Tech., **03** [04]181-188 (2012)
DOI: 10.4416/JCST2012-00018
available online at: http://www.ceramic-science.com

Surface Strengthening of Extrusion-Formed Polymer/Filler-Derived Ceramic Composites

L. Schlier*[1], N. Travitzky[1], J. Gegner[2], P. Greil[1]

[1]Department of Materials Science, (Glass and Ceramics), University of Erlangen-Nuernberg, Martensstr. 5, 91058 Erlangen, Germany
[2]Department of Material Physics, SKF GmbH, Gunnar-Wester-Str. 12, 97421 Schweinfurt, Germany
received June 4, 2012; accepted July 25, 2012

Abstract

Surface nitridation of extrusion-formed Fe-Si-Cr-filler-loaded polysiloxane polymer filaments was investigated. After the filaments were exposed to a nitrogen atmosphere at temperatures above 1000 °C, a gas-solid reaction caused the formation of a nitridation reaction layer covering the filament surface. Thermo-chemical calculations of equilibrium phase compositions at different nitrogen activity suggest the formation of Si_2N_2O and Si_3N_4 near the filament surface (high nitrogen content) whereas SiC and unreacted $CrSi_2$ and FeSi dominate in the core region (low nitrogen content), which was confirmed by means of XRD analyses. Compared to filaments annealed in an inert Ar atmosphere (no nitride reaction layer), specimens covered with a nitride surface layer of only 20 μm in thickness obtained a bending strength increment of + 35 % (mean fracture stress 400 MPa). The improved mechanical properties were attributed to a pronounced volume increase triggered by the nitride reaction, which gives rise to pore filling and crack healing. Since post-fabrication treatment in a reactive atmosphere is independent of the component shape and size, formation of a surface reaction zone with densified microstructure (reduced porosity and flaws) may offer a versatile route for improving the properties of bulk polymer-filler-derived ceramic components.

Keywords: Polymer derived ceramics, surface strengthening, reaction surface zone

I. Introduction

Polymer-derived ceramics (PDCs) were developed from a number of organo-silicon and organo-silicon-boron polymer precursors which upon thermal decomposition in an inert atmosphere (pyrolysis) yield ceramics in the systems Si-C-N-B-O [1]. PDCs with variable composition and an amorphous or crystalline microstructure were reported to offer excellent thermal stability [2] as well as interesting electric, piezoelectric, magnetic, optical and chemical properties [1]. The mechanical and tribological properties of PDCs and PDC-based composites may vary in a wide range. Maximum values for Young's modulus of 155 GPa, Vickers hardness of 26 GPa, fracture toughness of 3 $MPam^{1/2}$, and fracture strength of 1100 MPa can be found in the literature [3]. A superior creep resistance at temperatures even exceeding 1500 °C observed in Si-(B)-C-N-based PDCs [4] was attributed to the evolution of a nanodomain network of graphene that was hypothesized to support stress even at very high temperatures [5]. These property values, however, were often measured on specimens with a very small volume (a few mm^3) or low dimensionality (fibres, layers with thickness < 1 mm) with the application of nanotechniques. Current applications are therefore mainly limited to low-dimensional product shapes such as high-temperature-resistant fibres [6,7], coatings [8], joints and seals [9], micro- and macrocellular foams [10], sensor sheets [11] and micro electro-mechanical systems (MEMS) [12].

Enhancement of mechanical properties in bulk components with larger volume is hampered mainly by the problem of controlling the nano- and microstructure formation process under the constraints of limited transport of gaseous decomposition products and retardation of strain relaxation upon polymer-to-ceramic conversion. Since polymer-to-ceramic conversion involves a pronounced increase in density by a factor of 2 – 3 and a volumetric shrinkage that may exceed 50 %, porosity and crack formation are difficult to avoid in bulk-polymer-derived ceramic products [13]. Introducing non-reactive and reactive fillers that are able to compensate for the volume dilatation of the polymer phase with an appropriate expansion of a filler reaction phase successfully demonstrated near-net shape processing of complex-shaped polymer-derived functional components [14]. Loading of the polymeric precursor with solid filler powder (particles or fibres), however, may give rise to an increase in viscosity, which is likely to retard densification based on viscous flow (e.g. < 600 – 700 °C) and sintering (> 600 – 700 °C) required to achieve elimination of transient porosity upon polymer-to-ceramic conversion [15]. Reduction of residual porosity was achieved by application of stress-assisted consolidation techniques including pressure casting [3], warm-

* Corresponding author: lorenz.schlier@ww.uni-erlangen.de

pressing [16], field-assisted hot pressing [17], and hot isostatic pressing [18].

The emphasis of the current work is to explore densification of a surface-near zone as a result of annealing the extrusion-fabricated PDC in a reactive atmosphere (nitrogen) without applying any stress loading technique. A nitride phase reaction zone was formed on the surface of FeSiCr-filler-loaded polysilsesquioxane specimens, which gives rise to an improvement of the mechanical properties compared to untreated material. Supported by thermochemical calculations of solid-gas phase interaction, suitable processing conditions were identified. Since post-fabrication treatment in a reactive atmosphere is independent of the component shape and size, formation of a surface reaction zone with reduced porosity and flaws may offer a versatile route for improving the properties of bulk PDC components.

II. Experimental Procedure

(1) Raw materials

A feedstock applied for extrusion shaping was prepared from a polymethylsilsesquioxane ($[CH_3SiO_{1.5}]_{\sim 140}$ (PMS, molecular weight $M_w = 9400$ g/mol)) (Silres MK, Wacker Chemie AG, Burghausen, Germany) with a melting temperature of 55 °C, and a typical cross-linking temperature of 200 °C (2 h). The polymer precursor powder was mixed with two types of filler: ferro-silicochromium (FeSiCr) powder (FeSiCr 150, MLR GmbH Co. KG, Leun, Germany) and SiC (SiC UF05 green, H.C. Starck, Selb, Germany). While FeSiCr served as a reactive filler component to facilitate near-net shaping and pyrolytic consolidation [14], SiC loading improves the wear resistance of pyrolysed components.

(2) Extrusion forming

Extrusion forming of filler-loaded polymer feedstock requires control of cross-linking-induced viscosity variation within the time period of melting, transport and extrusion shaping. Based on rheological measurements of different feedstock compositions, a selected composition containing volume fractions of 0.5 PMS and 0.5 filler powder was prepared by mixing for 24 h in a ball mill filled with zirconia balls. Disc-shaped specimens (diameter 25 mm and thickness 2.5 mm) were prepared for rheological characterization of the feedstock. Viscosity was measured on an oscillating rheometer (UDS 200 Paar-Physika Messtechnik GmbH, Radeburg, Germany) up to a temperature of 170 °C, applying a shear rate of $\sim 1\ s^{-1}$. In order to attain reasonable processing conditions for extrusion forming of the system under investigation (gelation time > 10 min, viscosity $< 10^4$ [Pa · s]) the feedstock powder mixtures were melted in a laboratory-scale twin-screw extruder (Rheomex, Thermo-Haake, Karlsruhe, Germany) at temperatures up to 160 °C. At higher temperatures, an accelerated cross-linking reaction induces viscosity to rise steeply with time periods too short for melting and extrusion process. Continuous filaments of spherical (diameter 5 mm) and rectangular (3.5 x 3.4 mm^2) cross-sectional shape were fabricated by applying an extrusion velocity of 1 mm/s.

(3) Pyrolysis and surface reaction

Segments with a length of 25 mm and 50 mm were cut from the extruded and cross-linked filaments and pyrolysed at 950 °C in flowing N_2 atmosphere at ambient pressure. At this temperature conversion of organic PMS phase to an amorphous SiOC ceramic residue was almost terminated after a dwell time of 2 h. Subsequently, the specimens were pyrolysed at temperatures of 1100 °C, 1200 °C, 1300 °C, and 1400 °C. During annealing in nitrogen atmosphere for 1.5 h, nitrogen penetrated into the porous pyrolysis residue and a nitridation reaction zone was formed on the surface. Three different sets of specimens were prepared for analyses of their mechanical properties: one set was used as-nitrided containing the surface reaction zone (denoted (P)), another set was ground after nitridation to remove the surface reaction zone (PG), and a third set was ground and subsequently post-treated in nitrogen atmosphere again applying similar temperature/time/pressure conditions as described above (PGP).

(4) Microstructure analysis and mechanical testing

Density of the pyrolysed and surface-treated specimens was determined according to the Archimedes principle based on measurement of their volume and weight. The porosity distribution gradient perpendicular to the specimen surface was derived based on image analysis of SEM micrographs (SEM Quanta 200, FEI, Hillsboro, OR). Cross-sections perpendicular to the surface were prepared and contrast differences between solid material and pores were converted to 8-bit black-and-white images and analyzed quantitatively (ImageJ 1.37v, NIH, Bethesda, MD). The elemental composition was analyzed by means of energy-dispersive X-ray analysis EDX (INCA x-sight TV A3, Oxford Instruments, GB). Crystalline phases were analyzed on the pyrolyzed and annealed filament rods with X-ray diffraction (Kristalloflex D500, Siemens, Mannheim, Germany), applying monochromatic CuKα radiation at a scan rate of 0.75 °/min over a 2θ range of 10 – 70 °.

The modulus of rupture was measured with the four-point bending method (Instron 4204, Instron Corp., Canton/MA, USA) using span distances of 10/20 mm and 20/40 mm, respectively. The tests were conducted in the displacement-controlled mode at the rate of 0.5 mm/sec. The peak load was used to calculate the fracture strength. Mean values were derived from at least twenty specimens. While specimens of set (P) were tested as-nitrided, e.g. no mechanical surface finishing, specimen sets (PG) and (PGP) were polished to a 6 μm finish. The modulus of elasticity was derived from longitudinal sound propagation velocity measurement (Impulse excitation technique, Buzz-o-Sonic, BuzzMac Software, Glendale/WI, USA). The hardness was measured on polished cross-sections with the Vickers indentation technique, applying a load of 5 kg for 10 s (Zwick 3212, Zwick, Ulm, Germany). Hardness values were recorded along a line perpendicular to the specimen surface with a distance of approximately 400 μm between two measurement points.

(5) Thermochemical calculations

Gas-solid reactions relevant for the interaction of the nitrogen atmosphere with the pyrolysed-filler-loaded SiOC material were calculated with thermochemical calculation software (HSC 4, Outo-tec Pori, Finland). Basic thermochemical c_p, *H, S,* and *G* data of gaseous (SiO, CO, N_2) and condensed substances (C, SiC, SiO_2, $CrSi_2$, FeSi, Cr_5Si_3, Cr_7C_3, Si_2N_2O, Si_3N_4, CrN, Fe_3C) considered in the calculations were taken from the integrated database. The Gibbs energy minimization technique is used to calculate the amount of chemical species when specified elements or compounds are reacted to reach the state of equilibrium at a given temperature of 1300 °C. While all other input species were kept constant, the nitrogen content was varied in order to account for the high nitrogen activity on the surface and the low nitrogen activity in the core region of the extruded filament bodies. Ideal gas phase and stoichiometric phase compositions of condensed substances were assumed. Since polymethylsilsesquioxane-polymer-derived amorphous SiO_xC_y residue tends to crystallize at temperatures exceeding 1100 – 1200 °C, a mixture of stoichiometric substances of SiO_2, SiC, and C was considered in the calculations. Assuming mass balance, molar fractions corresponding to the overall ceramic residue composition SiO_xC_y were calculated from

$$SiO_xC_y \rightarrow 0.5\ SiC + x/2\ SiO_2 + (x/2 + y - 1)\ C \qquad (1)$$

Inserting values for $x \approx 3/2$ and $y \approx 1/3$ [19], one mole of $SiO_{3/2}C_{1/3}$ corresponds to (0.54 SiO_2 + 0.17 SiC + 0.28 C) which was taken for the calculations. XRD analysis revealed the reactive FeSiCr filler to be mainly composed of $CrSi_2$ and ε-FeSi with a minor amount of $FeSi_2$ Thus, based on the elemental composition, the reactive filler component was approximated with a molar phase composition of 0.65 $CrSi_2$ + 0.35 FeSi. While N_2 pressure equals the external pressure on the surface (0.1 MPa), it may be assumed to be low in the core region (at least during the initial stage of exposure). Therefore, equilibrium calculations were performed based on variation of the N_2 content (*n*) at 1300 °C with the mole number of nitrogen *n* varying from 0 (core) to 1 (surface). The results were visualized as a phase reaction diagram, which displays the limits of stability of the substances versus N_2 content. Even though the calculations do not take into account kinetic aspects e.g. time-dependent variation of local fugacities of gaseous species owing to molecular diffusion, the results of the calculations may indicate general trends of phase evolution dependent on the gradient of nitrogen content from the surface to the core of the PDC filament specimens.

III. Results and Discussion

(1) Extrusion forming and pyrolysis

Continuous filaments were fabricated from filler-loaded polymer feedstocks at extrusion temperatures up to 160 °C. During pyrolysis, thermal degradation of the polymer caused weight loss and shrinkage (Fig. 1). A weight loss of 3.6 wt% was recorded upon polymer-to-ceramic conversion, which corresponds to a ceramic yield of the polymer precursor of approximately 84 wt%. On exposure of the specimens to a nitrogen atmosphere, the specimen weight increased by about 1 wt% at 1100 °C. Simultaneously, pronounced radial and longitudinal shrinkage was measured on the filaments, which indicates reduction of transient porosity as a result of viscous sintering [13]. While the inorganic pyrolysis residue contains a residual porosity of ~ 8.5 %, densification upon annealing in nitrogen caused the porosity to decrease to < 2 % in the core and to < 0.5 % on the surface of the filaments. At temperatures exceeding 1300 °C a massive weight loss and expansion of the filament diameter is observed. Carbothermal reduction of oxycarbide residue at temperatures above 1350 °C was reported to result in precipitation of crystalline SiC and a loss of CO and SiO, which gives rise to massive weight loss and pore formation [20].

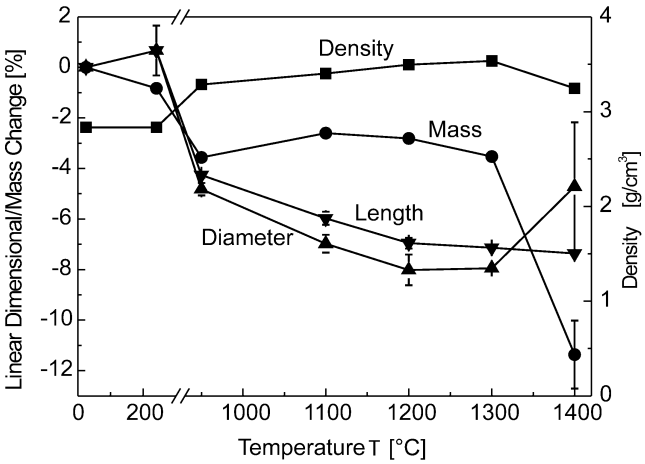

Fig. 1: Linear dimensional change and weight change during heat treatment in flowing nitrogen atmosphere.

XRD of the PDC filaments pyrolysed at 950 °C only reveals peaks of the filler powders (SiC, FeSiCr) (Fig. 2). The polymer-derived SiOC ceramic residue remains amorphous [21] and no reaction products of Cr or Fe were detected at this temperature. With increasing temperature, however, the reactive filler FeSiCr may undergo a sequence of carburization reactions. The presence of $Cr_5Si_3C_x$ found in the XRD spectra of specimens pyrolysed at 1200 °C indicates an intermediate state of carburization reaction [22], which might be represented by a tentative reaction sequence

$$\begin{aligned} &5\ CrSi_2 + 85/7\ C \\ &\rightarrow Cr_5Si_3C_x + (36-7x)/7\ C + 7\ SiC \\ &\rightarrow 5/7\ Cr_7C_3 + 10\ SiC \end{aligned} \qquad (2)$$

$$3\ FeSi + 4\ C \rightarrow Fe_3C + 3\ SiC \qquad (3)$$

which finally results in a mixture of carbide phases. The content of free carbon in the polymer pyrolysis residue is 28.6 mol%, which would be sufficient to convert only approximately 12 vol% of the FeSiCr filler fraction into Cr_7C_3, Fe_3C and SiC at least on the filler particle surfaces. Thus, the major part of the FeSiCr filler is likely to remain unreacted, as confirmed with XRD. Furthermore, previous work has shown that $CrSi_2$ needs reaction temperatures exceeding 1200 °C in inert atmosphere to undergo a carburization reaction with carbon precipitating from the polymer-derived Si-O-C(-H) residue [23].

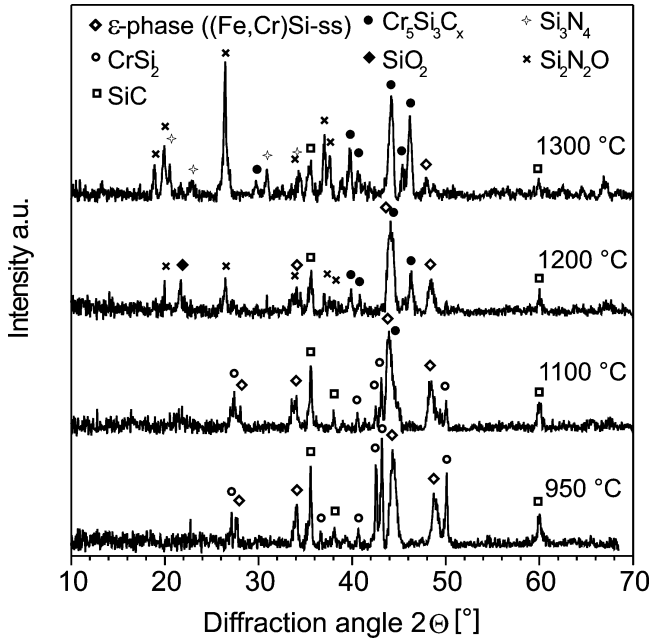

Fig. 2: XRD spectra of extruded filaments annealed in flowing nitrogen for 1.5 h at different temperatures.

(2) Surface nitridation reaction

Characteristic peaks of crystalline oxynitride and nitride species emerging after annealing in flowing nitrogen atmosphere at temperatures exceeding 1200 °C indicate the onset of the gas-solid surface reaction as reported from silicide-loaded polysiloxane systems [22]. At 1300 °C, Si_2N_2O is observed as the major reaction product with additional fractions of Si_3N_4 and $Cr_5Si_3C_x$, (Fig. 2). Cross-sections of the specimens annealed in flowing nitrogen atmosphere at ambient pressure for 1.5 h are shown in Fig. 3. While no distinct surface reaction layer can be detected on the specimen annealed at 1100 °C, a pronounced difference in contrast after annealing at 1300 °C reveals the formation of a nitride reaction layer with a thickness varying from 10 – 20 μm. After this reaction surface layer was removed by means of mechanical grinding and re-annealing at 1300 °C for 1.5 h, the reaction zone was reformed with the same thickness. Formation of a nitride reaction zone on the surface corresponds to an enrichment of the nitrogen concentration, which was measured by means of EDX (Fig. 4). Starting from a nitrogen concentration of approximately 25 at% on the surface, the nitrogen penetration depth extends to approximately 40 μm with the half width found at approximately 20 μm.

Different models were proposed to simulate the densification process caused by infiltration and reaction of vapour species into a porous specimen [24]. In these models, vapour species concentration along the infiltration direction is obtained by site- and time-dependent analysis of reaction rate and mass transfer (diffusion) assuming mass balance and different boundary conditions (constant pore radius – SP model; tapered pore radius – TP model, variation of pore size distribution – PC model). The models predicted the time variation of pore shapes, making it possible to predict threshold values for the transition of pore closure modes expressed by the Thiele modulus [25]. Assuming diffusion governs the penetration depth of the nitrided surface layer, which is reasonable at least in a later stage of the surface nitridation reaction, the variation of nitrogen concentration C_N with time t and surface distance x during exposure to nitrogen atmosphere may be approximated by solution of the 2nd Fick's law. For a plane source (surface) condition, C_N may be expressed by using the error function [26]

$$C_N = C_N^0 \left[1 - \mathrm{erf}\left(\frac{x}{2\sqrt{D_{eff}\,t}}\right)\right] \qquad (4)$$

C_N^0 is the initial concentration at time $t = 0$ and surface distance (depth) $x = 0$ and D_{eff} is the effective diffusion constant usually given as an Arrhenius law. Fitting Eq. (4) to the experimental data plotted in Fig. 4 results in an effective diffusion coefficient D_{eff} (1300 °C) of the order of 10^{-17} cm²/s. This value is three to four orders of magnitude larger than lattice diffusivity of N in α-Si_3N_4 and β-Si_3N_4 of $D_{Si_3N_4}$ (1300 °C) ≈ 2.2 x 10^{-20} cm²/s (α) and ≈ 9.1 x 10^{-20} cm²/s (β), respectively, as calculated from the Arrhenius law (D_N (α-Si_3N_4) = 1.2 x 10^{-12} exp (-233/RT) and D_N (β-Si_3N_4) = 5.8 x 10^6 exp (-777 /RT) with D_0 given in [cm²/s] and Q* in [kJ/mol]) [27]. Residual porosity (0.5 %) and grain boundaries may give rise to enhanced diffusion of nitrogen.

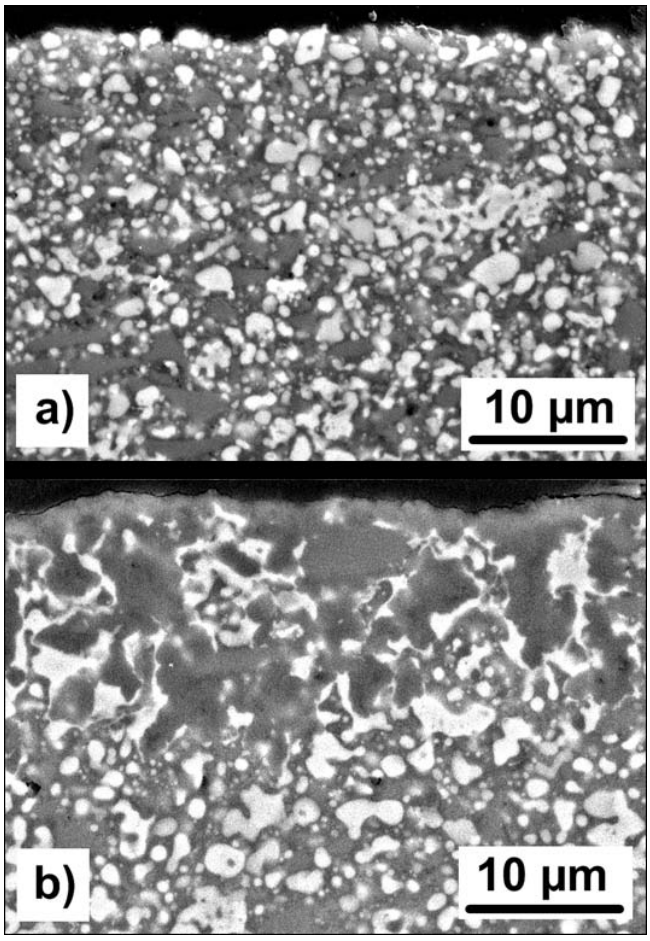

Fig. 3: Microstructure of specimens annealed in flowing nitrogen for 1.5 h at 1100 °C (a) and 1300 °C (b) (polished cross-sections perpendicular to surface).

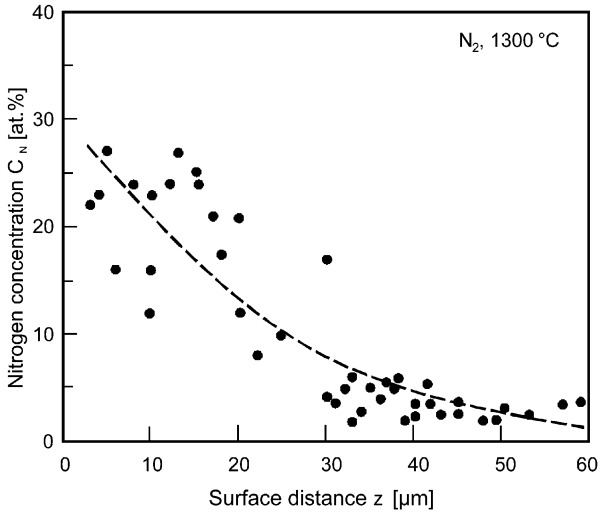

Fig. 4: Nitrogen distribution perpendicular to surface measured by EDX.

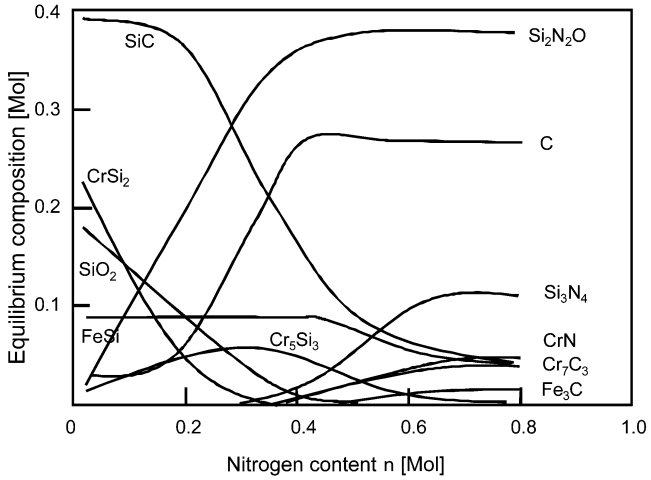

Fig. 5: Thermochemical equilibrium composition calculations (1300 °C, pN_2 0.1 MPa) showing the condensed phase composition as a function of the nitrogen content.

Thermochemical calculations were performed, taking the feedstock composition as input values, to evaluate equilibrium compositions predicted for the reaction zone at different nitrogen concentrations. In order to account for a difference in nitrogen content from the surface to the core region, the nitrogen content was varied from 0 to 1 mole N_2. Fig. 5 shows the results of thermochemical calculations for a reaction temperature of 1300 °C and a nitrogen vapour pressure of 0.1 MPa. While in the core region the equilibrium composition is represented by a mixture of SiC – SiO_2 – $CrSi_2$ – FeSi, major constituents predicted in the nitrided reaction zone (surface) are Si_2N_2O – C – Si_3N_4. Although the thermochemical calculations do not take into account kinetic aspects and reaction mechanisms, the results coincide well with the phase composition determined experimentally by means of XRD and SEM (EDX) on the filament surface. Earlier work on the nitridation of elemental Si has shown that reaction of Si with nitrogen may be catalyzed by a metal element [28]. Lower reaction temperatures and shorter reaction time were reported for $MeSi_2$ with the relative catalytic effect increasing for metal Me from Va to VIII period in the periodical element system [22]. Catalytic nitridation was attributed either to the formation of low-melting metal-silicon eutectics (Fe-Si: $T_{eu} \approx 1200$ °C; Cr-Si: $T_{eu} \approx 1315$ °C) [29] and to dissociative chemisorption of molecular nitrogen on the metal particle surface [30]. Both Cr and Fe were found to catalyze the nitridation reaction of Si effectively at reaction temperatures as low as 1100 °C [31]. Furthermore, catalytic nitridation was reported to favour formation of Si_3N_4 owing to enhanced mobility of atomic nitrogen [32].

(3) Surface microstructure modification and mechanical properties

Substantial changes in the microstructure may be correlated to the specific volume expansion associated with the nitridation reaction. Taking the phase contents derived from the calculated composition, the volume changes associated with the nitridation reaction were derived based on the rule of mixtures

$$\frac{\Delta V}{V_c}(n) = \frac{\sum_i \nu_i \Omega_i(n)}{\sum_i \nu_i \Omega_i(n=0)} \qquad (5)$$

where V_c is the total volume of the core composition (n = 0) and ν_i and Ω_i denote the mole numbers and molar volumes of species (i), Fig. 6 shows the estimated volume expansion, $\Delta V/V_c$, of the phase compositions calculated as a function of the N_2 content. For the case of complete nitridation (surface after long exposure period) a maximum volume expansion of approximately 40 % compared to the core composition is derived. Thus, in the region of nitridation reaction, volume expansion may give rise to a reduction of porosity and a healing of cracks. In order to demonstrate the healing capacity a microindent crack pattern was prepared by means of Vickers indentation on a pyrolysed and ground filament surface. After annealing in flowing nitrogen at 1300 °C for 2 h, the radial indent cracks were completely filled with nitride reaction product (Fig. 7). In the open crack, carbothermal reduction is likely to form Si_3N_4 [33]

$$3\,SiO\,(g) + 3\,C\,(s) + 2\,N_2\,(g) \rightarrow Si_3N_4\,(s) + 3\,CO\,(g) \qquad (6)$$

which reduces the carbon content near the surface. The pronounced volume increase of this reaction of $\Delta V/V_C = +118$ % promotes closure of open cracks and pores. For this case, volume increase is compensated by linear expansion perpendicular to the surface only, e.g. lateral expansion is restricted, the maximum crack opening d_{op} to be filled by the nitridation reaction product is given by

$$d_{op} = 2x\left[\frac{\Delta V}{V_c} - 1\right] \qquad (7)$$

Thus for x(1300 °C, 1.5 h) ≈ 20 µm cracks and large pores with a maximum opening of approximately $d_{op} \approx 16$ µm are expected to be filled with the nitride reaction product resulting from the thermochemical calculations (and $d_{op} \approx 47$ µm for Si_3N_4 formation according to Eq. (7)). Analysis of cross-sections prepared perpendicular to the surface revealed that the indent crack shown in Fig. 7 was completely filled with nitride reaction product even at a surface distance of 50 µm.

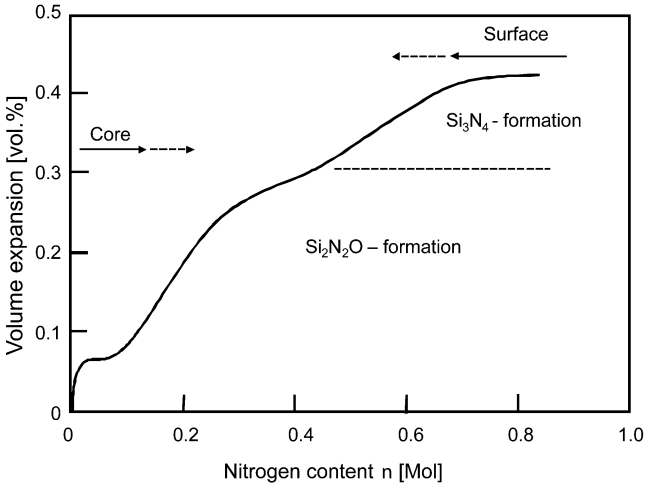

Fig. 6: Volume expansion calculated from the equilibrium compositions shown in Fig. 5.

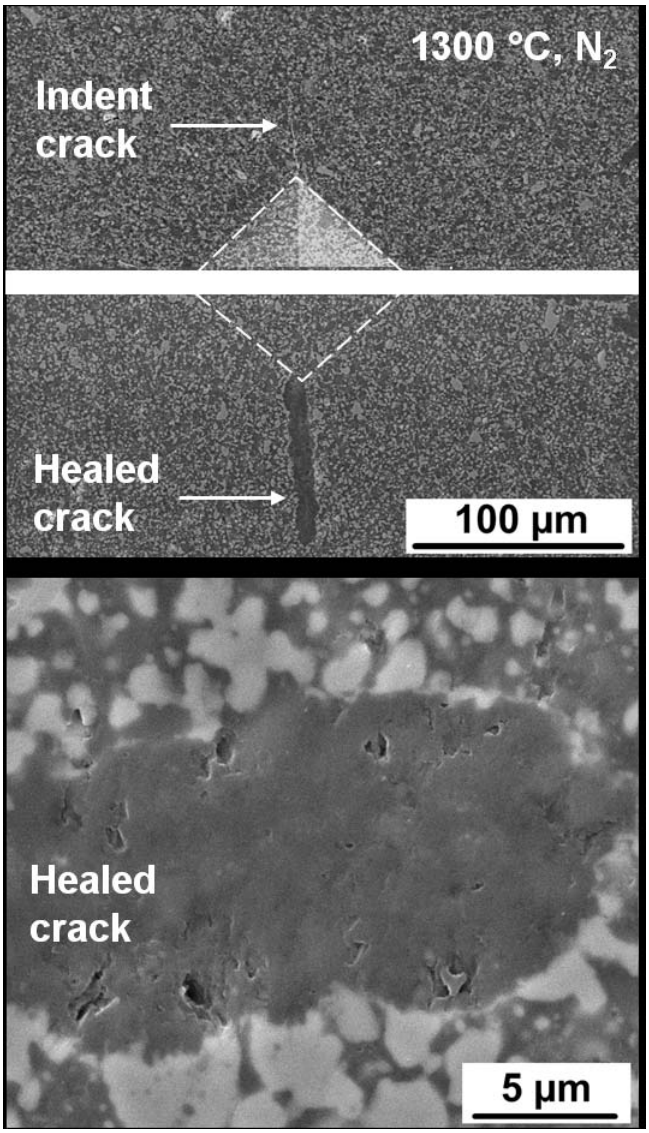

Fig. 7: Vickers indent crack and crack healing after nitrogen surface reaction at 1300 °C.

Experimental measurements of porosity distribution confirm the trend of porosity gradient formation upon nitridation treatment. Near the surface a minimum porosity of less than 0.5 % compared to 1 – 2 % in the core region was determined after annealing at 1300 °C (Fig. 7). Porosity reduction and healing of surface cracks during annealing in nitrogen atmosphere give rise to a pronounced increase in hardness (Fig. 8). Hardness of the porous region scales with the increase of density from the core to the surface and reached a maximum value of 11.8 GPa. This value is only slightly lower than hardness values measured for CVD- and PVD-deposited Si_3N_4 and hot-pressed Si_2N_2O (12 – 19 GPa) [34, 35], suggesting that the outer surface is dominated by nitride-rich phase composition.

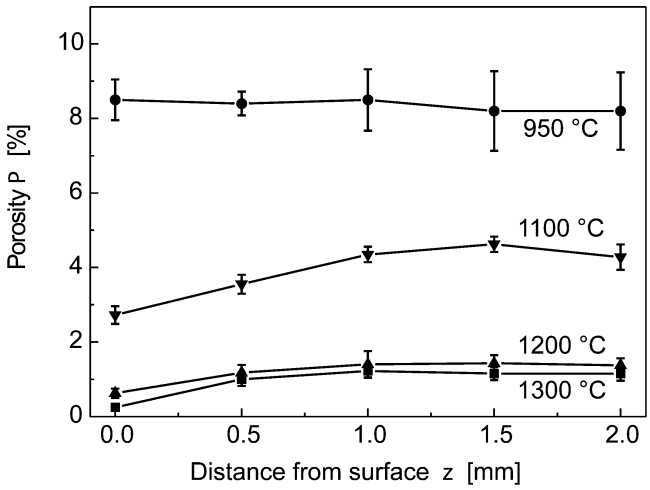

Fig. 8: Radial porosity distribution of pyrolysed filaments after annealing in flowing N_2-atmosphere at different temperatures.

Fig. 9 shows the fracture stress values measured on the pyrolysed filaments after annealing in nitrogen atmosphere at various temperatures. After the surface layer was removed by grinding, the resulting bending strength of the core material shows an increase from 170 MPa (950 °C) to 260 MPa (1300 °C). The bending strength measured on samples after nitridation treatment and without surface finishing reaches values up to 400 MPa (1300 °C). Filling of pores and healing of cracks accessible to the nitrogen atmosphere by Si_2N_2O and Si_3N_4 reaction products may be considered as a potential mechanism for reduction of defect size as well as enhancement of fracture toughness, giving rise to the improvement of fracture stress by approximately + 35 %. Compared to the low level of fracture toughness of 1 – 2 $MPam^{1/2}$ associated with the porous and amorphous microstructure of the polymer-derived ceramic residue [1], formation of dense crystalline oxynitride/nitride surface layers may attain significantly higher toughness ranging from 3 (Si_2N_2O) to > 6 $MPam^{1/2}$ (Si_3N_4) [35, 36]. Healing of machining defects in silicon nitride (gas-pressure-sintered with Y_2O_3 and Al_2O_3) was achieved by annealing at 1000 °C in air, which caused a pronounced increase in strength of 300 to 500 MPa (corresponding to 20 – 40 %) [37]. The improvement was attributed to the formation of a small (0.5 – 2 µm) glassy silica layer oxidation product which filled surface cracks and surface-related pores during annealing. As we were able to demonstrate, surface nitridation treatment may effectively trigger healing of open cracks at 1300 °C without forming low-viscous oxide products, which might be of interest for improved wear stability at elevated temperatures.

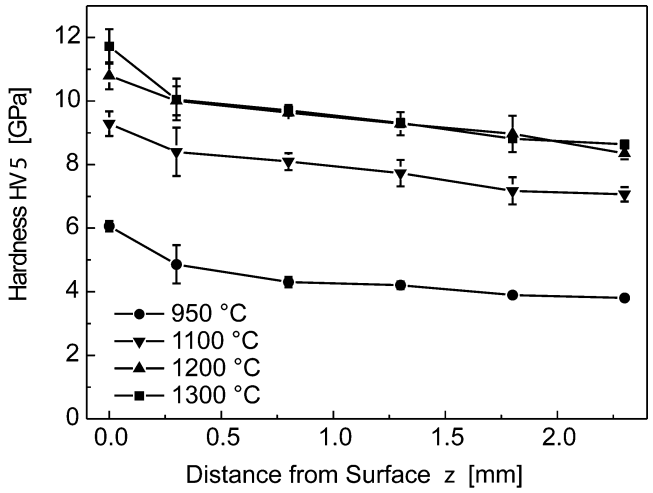

Fig. 9: Radial hardness distribution of pyrolysed filaments after annealing in flowing N_2-atmosphere at different temperatures.

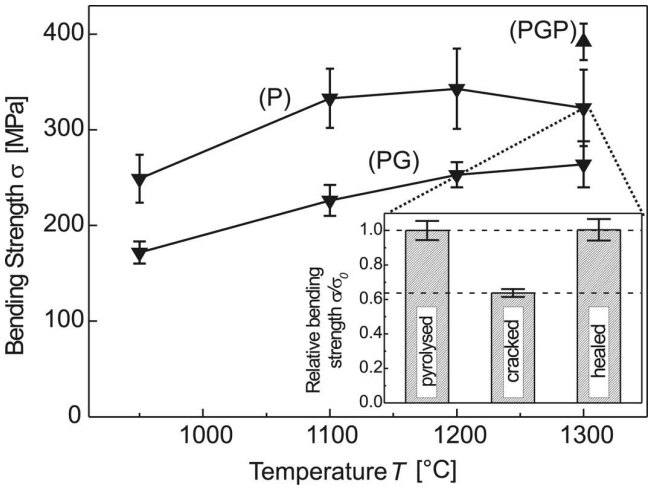

Fig. 10: Bending strength measured after pyrolysis at 950 °C (N_2) and subsequent annealing in N_2-atmosphere for 2 h at various temperatures (P), after removal of the reaction layer by grinding (PG) and after subsequent re-annealing at the same temperature (PGP) for different binder contents and post-treatments after pyrolysis.

V. Conclusions

Surface nitridation was demonstrated to yield improved mechanical properties of extrusion-formed preceramic polymer-derived ceramic composites. We found that a thin layer (< 20 μm) of oxynitride/nitride reaction product was sufficient to effect a strength increment of approximately + 35 %. The pronounced improvement is believed to originate from the formation of a gradient microstructure with a dense (porosity < 0.5 %) surface layer dominated by a Si_2N_2O/Si_3N_4 reaction product layer that covers the porous core region of the filaments composed of SiOC residue and unreacted filler (FeSiCr). While earlier work referred to nitridation applying significantly higher nitrogen pressure up to 10 MPa [14], we demonstrated that a flowing nitrogen atmosphere at ambient pressure (0.1 MPa) was effective in the reduction of surface porosity and healing of surface cracks. Further improvement may be expected based on optimization of the heat treatment, precursor composition and nitride surface layer thickness. Since post-fabrication treatment in a reactive atmosphere is independent of the component shape and size, formation of a surface reaction zone with optimized microstructure (reduced porosity and flaws) may offer a versatile route for improving the properties of bulk PDC components.

Acknowledgements

Financial support from the DFG-funded Koselleck project GR 961/32 and from SKF GmbH is gratefully acknowledged.

References

1 Colombo, P., Mera, G., Riedel, R., Sorarù, G.D.: Polymer-derived ceramics: 40 years of research and innovation in advanced ceramics, *J. Am. Ceram. Soc.*, **93**, 1805 – 1837, (2010).

2 Riedel, R., Kienzle, A., Dressler, W., Ruwisch, L., Bill, J., Aldinger, F.: A silicoboron carbonitride ceramic stable to 2 000 °C, *Nature*, **382**, 796 – 798, (1996).

3 Shah, S.R., Raj, R.: Mechanical properties of a fully dense polymer derived ceramic made by a novel pressure casting process, *Acta Mater.*, **50**, 4093 – 4103, (2002).

4 Kumar, R., Prinz, S., Cai, Y., Zimmermann, A., Aldinger, F., Berger, F., Müller, K.: Crystallization and creep behaviour of Si-B-C-N ceramics, *Acta Mater.*, **53**, 4567 – 4578, (2005).

5 Saha, A., Williamson, D.L., Raj, R.: A model for nano domains in polymer-derived SiCO, *J. Am. Ceram. Soc.*, **89**, 2188 – 2195, (2006).

6 Ishikawa, T., Kohtoku, Y., Kumagawa, K., Yamamura, T., Nasagawa, T.: High-strength alkali-resistant sintered SiC fibre stable up to 2 200 °C, *Nature*, **391**, 773 – 775, (1998).

7 Bunsell, A.R., Piant, A.: A review of the development of three generations of small diameter silicon carbide fibres, *J. Mater. Sci.*, **41**, 823 – 839, (2006).

8 Torrey, J.D., Bordia, R.K.: Mechanical properties of polymer-derived ceramic composite coatings on steel, *J. Europ. Ceram. Soc.*, **28**, 253 – 257, (2008).

9 Lewinsohn, C.A., Elangovan, S.: Development of amorphous, non-oxide seals for solid oxide fuel cells, *Ceram. Eng. Sci. Proc.*, **24**, 317 – 322, (2003).

10 Colombo, P.: Engineering porosity in polymer-derived ceramics, *J. Eur. Ceram. Soc.*, **28**, 1389 – 1395, (2008).

11 Nagaiah, N.R., Kapat, J.S., An, L., Chow, L.: Novel polymer derived ceramic-high temperature heat flux sensor for gas turbine environment, *J. Phys.: Conf. Ser.*, **34**, 458 – 463, (2006).

12 Liew, L., Zhang, W., Bright, V.M., An, L., Dunn, M.L., Raj, R.: Fabrication of SiCN ceramic MEMS using injectable polymer-precursor technique, *Sensors and Actuators: A. Physical*, **89**, 64 – 70, (2001).

13 Greil, P.: Net shape manufacturing of polymer derived ceramics, *J. Europ. Ceram. Soc.*, **18**, 1905 – 1914, (1998).

14 Greil, P.: Active filler controlled pyrolysis of preceramic polymers (AFCOP), *J. Am. Ceram. Soc.*, **78**, 835 – 48, (1995).

15 Sanchez-Jimenez, P.E., Downs, J.A., Raj, R.: Transient viscous flow during the evolution of a ceramic (silicon carbonitride) from a polymer (polysilazane), *J. Am. Ceram. Soc.*, **93**, 2567 – 2570, (2010).

16 Li, Y.L., Fan. H., Su, D., Fasel, C., Riedel, R.: Synthesis, structure, and properties of bulk Si(O)C ceramics from polycarbosilazane, *J. Am. Ceram. Soc.*, **92**, 2175 – 2181, (2009).

17 Esfehanian, M., Oberacker, R., Fett, T., Hoffmann, M.J.: Development of dense filler-free polymer-derived SiOC ceramics by field-assisted sintering, *J. Am. Ceram. Soc.*, **91**, 3803 – 3805, (2008).

18 Ishihara, S., Gu, H., Bill, J., Aldinger, F., Wakai, F.: Densification of precursor-derived Si-C-N ceramics by high-pressure hot isostatic pressing, *J. Am. Ceram. Soc.*, **85**, 1706 – 1712, (2002).

[19] Scheffler, M., Gambaryan-Roisman, T., Takahashi, T., Kaschta, J., Muenstedt, H., Buhler, P., Greil, P.: Pyrolytic decomposition of organo polysiloxanes, *Ceram. Trans.*, **115**, 239 – 250, (2000).

[20] Belot, V., Corriu, R.J.P., Leclerq, D., Mutin, P.H.,Vioux, A.: Silicon oxycarbide glasses with low O/Si ratio from organosilicon precursors, *J. Non-Crystall. Sol.*, **176**, 33 – 44, (1994).

[21] Hurwitz, F.I., Heimann, P., Farmer, S.C., Hembree, D.M.: Characterization of the pyrolytic conversion of polysilsesquioxanes to silicon oxycarbides, *J. Mat. Sci.*, **28**, 6622 – 6630, (1993).

[22] Erny, T.: Formation and properties of polymer derived composite ceramics of the system $MeSi_2$/polysiloxane, PhD Thesis, Univ. Erlangen-Nuernberg, Germany (1996).

[23] Schiavon, M.A., Yoshida, I.V.P.: Ceramic matrix composites derived from $CrSi_2$-filled silicone polycyclic network, *J. Mat. Sci.*, **39**, 4507 – 4514, (2004).

[24] Yoshikawa, N., Evans, J.W.: Modeling of chemical vapor infiltration rate considering a pore size distribution, *J. Am. Ceram. Soc.*, **85**, 1485 – 1491, (2002).

[25] Levenspiel, O.: Chemical reaction engineering, 2nd Ed.; pp. 469 – 74. Wiley, New York, (1972).

[26] Crank, J.: The Mathematics of diffusion, Oxford Univ. Press, UK, (2004).

[27] Petzow, G., Herrmann, M.: Silicon nitride ceramics, in Jansen "Structure and Bonding" Vol. 102, Springer Verl. Berlin, 47 – 168, (2002).

[28] Lin, S.: Comparative studies of metal additives on the nitridation of high purity silicon, *J. Am. Ceram. Soc.*, **60**, 78 – 81, (1977).

[29] Moulson, A.J.: Review: RBSN – its properties and formation, *J. Mat. Sci.*, **14**, 1017 – 1051, (1979).

[30] Bond, G.C.: Heterogeneous catalysis: Principles and applications, Oxford University Press, (1974).

[31] Cofer, C.G., Lewis, J.A.: Chromium catalysed silicon nitridation, *J. Mat. Sci.*, **29**, 5880 – 5886, (1994).

[32] Pigeon, A., Varma, A., Miller, A.: Some factors influencing the formation of reaction-bonded silicon nitride, *J. Mat. Sci.*, **28**, 1919 – 1936, (1993).

[33] Durham, S.J.P., Shanker, K., Drew, R.A.L.K.: Carbothermal synthesis of silicon Nitride: effect of reaction conditions, *J. Am. Ceram. Soc.*, **74**, 31 – 37, (1991).

[34] Xiao, Z.G., Mantei, T.D.: Plasma-enhanced deposition of hard silicon nitride-like coatings from hexamethyldisiloxane and ammonia, *Surf. Coat. Tech.*, **172**, 184 – 188, (2003).

[35] Larker, R.: Reaction sintering and properties of silicon oxynitride densified by hot isostatic pressing, *J. Am. Ceram. Soc.*, **75**, 62 – 66, (1992).

[36] Riley, F.L.: Silicon nitride and related materials, *J. Am. Ceram. Soc.*, **83**, 245 – 265, (2000).

[37] Harrer, W., Danzer, R., Morell, R.: Influence of surface defects on the biaxial strength of a silicon nitride ceramic – increase of strength by crack healing, *J. Eur. Ceram. Soc.*, **32**, 27 – 35 (2012).